Structural and electronic properties of NbN/GaN junctions grown by molecular beam epitaxy

Cite as: APL Mater. 10, 051103 (2022); doi: 10.1063/5.0083184
Submitted: 22 December 2021 • Accepted: 8 April 2022 •
Published Online: 3 May 2022

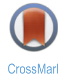

John G. Wright,[1,a)] Celesta S. Chang,[2] David A. Muller,[3,b)] Huili G. Xing,[1,4,b)] and Debdeep Jena[1,4,b)]

AFFILIATIONS

[1] Department of Materials Science and Engineering, Cornell University, Ithaca, New York 14853, USA
[2] Research Laboratory of Electronics, Massachusetts Institute of Technology, Cambridge, Massachusetts 02139, USA
[3] Department of Applied and Engineering Physics, Cornell University, Ithaca, New York 14853, USA
[4] School of Electrical and Computer Engineering, Cornell University, Ithaca, New York 14853, USA.

[a)] **Author to whom correspondence should be addressed:** jgw92@cornell.edu
[b)] **Also at:** Kavli Institute for Nanoscale Science, Cornell University, Ithaca, New York 14853, USA.Also at: Kavli Institute for Nanoscale Science, Cornell University, Ithaca, New York 14853, USA.

ABSTRACT

We report the structural and electronic properties of NbN/GaN junctions grown by plasma-assisted molecular beam epitaxy. High crystal-quality NbN films grown on GaN exhibit superconducting critical temperatures in excess of 10 K for thicknesses as low as 3 nm. We observe that the NbN lattice adopts the stacking sequence of the underlying GaN and that domain boundaries in the NbN thereby occur at the site of atomic steps in the GaN surface. The electronic properties of the NbN/GaN junction are characterized using Schottky barrier diodes. Current–voltage–temperature and capacitance–voltage measurements are used to determine the Schottky barrier height of the NbN/GaN junction, which we conclude is ~1.3 eV.

© 2022 Author(s). All article content, except where otherwise noted, is licensed under a Creative Commons Attribution (CC BY) license (http://creativecommons.org/licenses/by/4.0/). https://doi.org/10.1063/5.0083184

I. INTRODUCTION

Epitaxial heterostructures incorporating superconducting and metallic transition metal nitrides (TMNs) with III-nitride semiconductors have applications in Josephson junction qubits,[1,2] high frequency acoustic filters,[3,4] thermionic and plasmonic metamaterials,[5–7] novel topological electron systems,[8] and perhaps unforeseen new structures enabled by broadening the design space.

NbN is one of the several TMN materials that crystallize in a cubic rocksalt crystal structure, in contrast to the hexagonal wurtzite GaN and AlN crystals. Despite the structural dissimilarity between the two families of materials, heteroepitaxy of rocksalt TMNs and wurtzite III-N semiconductors is possible[9] as a result of similar metal–metal bond lengths and the similarity between the close-packed cation sublattices of the two crystal structures. This becomes particularly apparent when the stacking sequence of the cubic crystal along the body-diagonal is compared with that of the hexagonal crystal about the c-axis.

Previous reports have demonstrated the growth of NbN/III-N structures.[8–10] In reports of Yan *et al.* and Dang *et al.*, an AlN/GaN high-electron-mobility transistor is grown on a superconducting NbN film. Although this specific structure is interesting for several reasons, we highlight it here primarily as a proof that high quality III-N/TMN heteroepitaxy is possible. This ability to integrate metallic and superconducting NbN layers into III-N structures can enable the design of new electronic, optoelectronic, and acoustic devices that leverage the exceptional properties of both materials.

The fabrication and applications of epitaxial metal/semiconductor heterostructures have been investigated previously using both cubic III-As[11,12] and rocksalt III-N materials.[13] In this report, we aim to develop knowledge of the growth and electronic properties of wurtzite III-N/TMN heteroepitaxial structures.

It is with this motivation in mind that we study the epitaxial growth of NbN on GaN. We observe that coherent epitaxy of NbN on GaN is possible below a critical thickness between 3 and 6 nm. Above this thickness, we find that NbN films grown on GaN become granular. NbN films grown on GaN maintain high superconducting critical temperatures of $T_c \geq 10$ K for film thicknesses down to about 3 nm. The engineering of future III-N/TMN

heteroepitaxial structures and devices will require knowledge of the electronic properties of the interface between the different materials, such as the energy offset between the III-N conduction band and the TMN Fermi level. To this end, we have studied the electronic properties of the NbN/GaN junction and determined the Schottky barrier height at the NbN/GaN interface to be approximately Φ_B^{CV} = 1.38 eV.

II. RESULTS

A. Structural properties of the NbN films

Figure 1(a) shows atomic force microscopy (AFM) surface height maps, and Fig. 1(b) shows the reflection high energy electron diffraction (RHEED) patterns of NbN films grown on GaN as a function of NbN thickness. We observe that NbN films of ~3 nm in thickness possess the same terraced morphology of the underlying GaN film, with atomic step heights that correspond with the ~2.5 Å (1 1 1) interplanar spacing of the NbN. As the NbN film thickness is increased beyond 3 nm, we see in Fig. 1(a) increasing film roughness and a transition to a granular surface structure. Specifically, for the 5.8 nm NbN film, the AFM surface height map reveals decoration of the step edges with islands, while the underlying terraced structure is maintained. Figure 1(b) shows that the RHEED patterns become increasingly spotty as the thickness increases, confirming the transition to a granular surface structure.

As shown in Fig. 1(c), oscillations of the RHEED specular spot are observed upon nucleation of the NbN, indicating a layer-by-layer growth mode that persists for ~12 monolayers, or about 3 nm. This corresponds well with the observation that as the NbN thickness is increased beyond 3 nm, the AFM surface maps reveal an increasingly granular film structure, corresponding with a transition to an island growth mode.

Measurements of the resistance vs temperature [Fig. 1(d)] for different NbN films allow extraction of the superconducting transition temperature of the NbN on GaN films [Fig. 1(e)], which shows that down to ~3 nm, the films show only small decreases of the transition temperature relative to thicker NbN films, but below this thickness, transitions to the superconducting state are not observed above 2 K. This coincides with nearly constant film resistivity as a function of thickness down to 3 nm, followed by large increases in film resistivity [Fig. 1(f)] for films below 3 nm in thickness, which

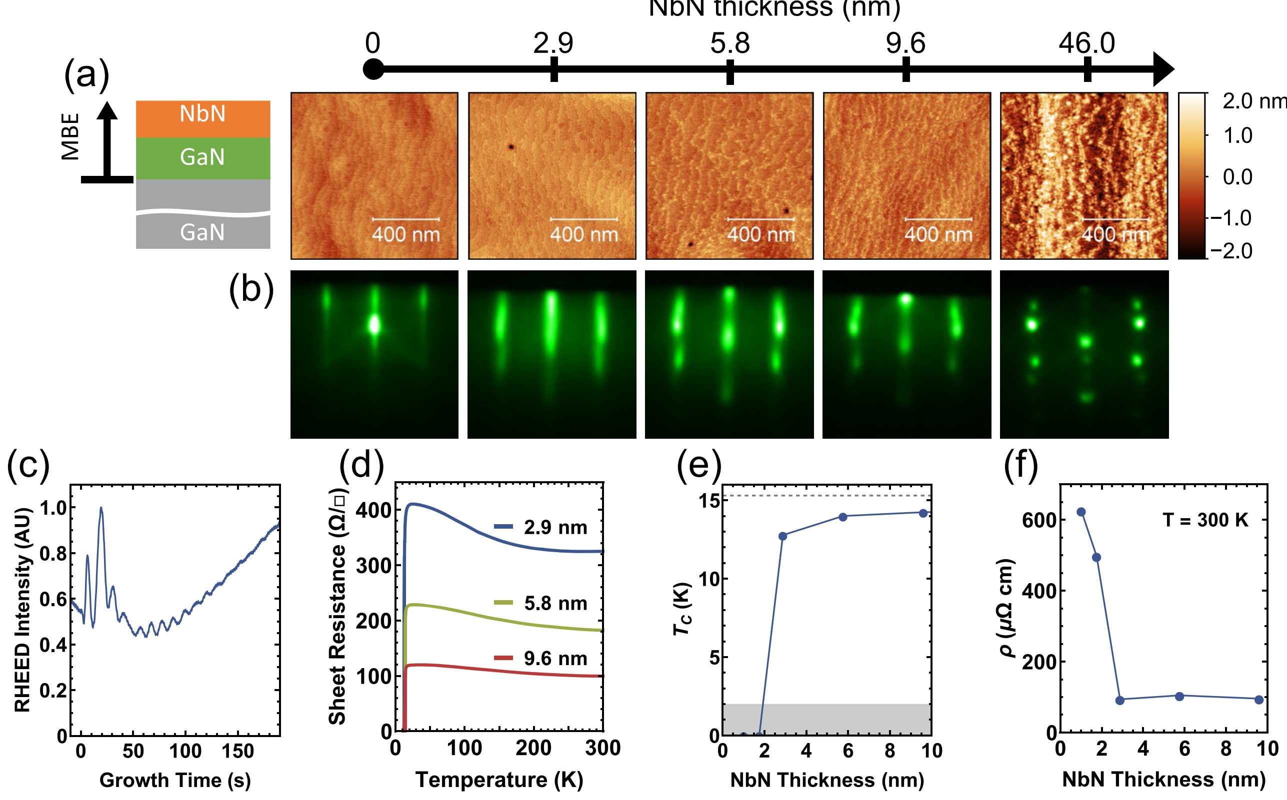

FIG. 1. (a) 1 × 1 μm^2 AFM surface height maps for NbN films of different thicknesses. (b) *In situ* post-growth RHEED patterns. (c) *In situ* RHEED specular spot peak intensity oscillations as a function of time throughout the first 200 s of growth of NbN. (d) Sheet resistance as a function of temperature for NbN films of different thicknesses. (e) Superconducting transition temperature of NbN as a function of thickness. The dashed horizontal line represents the measured critical temperature for a 46 nm NbN film. The minimum measurement temperature was 1.8 K, represented by the gray region of the plot. (f) Room temperature normal state resistance of NbN films as a function of thickness.

© Author(s) 2022

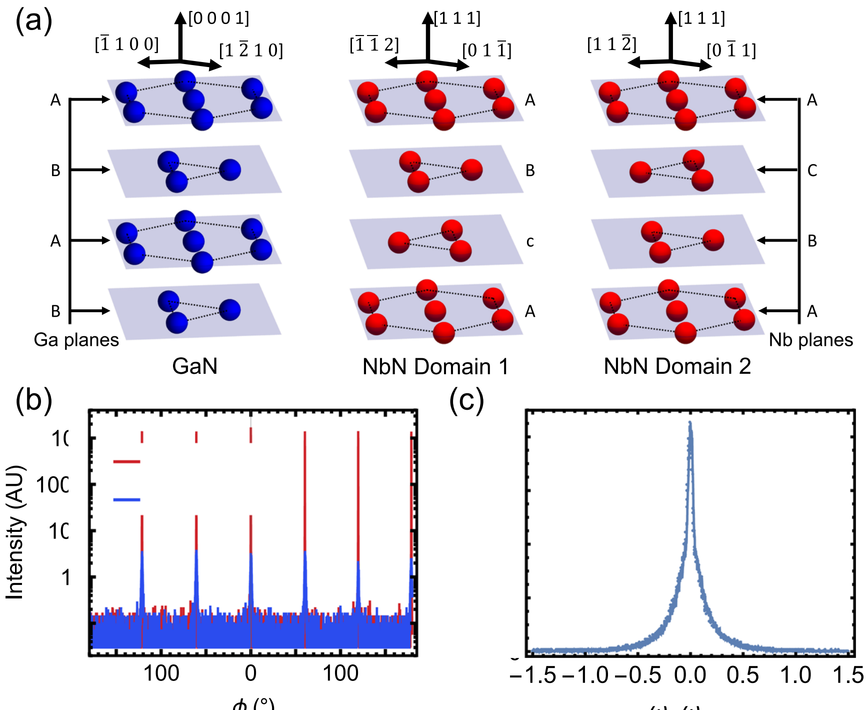

FIG. 2. (a) The cation lattices of GaN and NbN, as well as the relative lattice orientations of NbN and GaN. (b) XRD asymmetric ϕ-scan of both GaN and NbN revealing the in-plane alignment of both films. (c) XRD rocking curve of the out-of-plane NbN (1 1 1) peak for a 46 nm NbN film, with a FWHM = 291.

we hypothesize is due to oxidation of the NbN film upon exposure to air.

Previous reports of NbN growth on c-axis oriented GaN[10] and other hexagonal substrates, such as 6H-SiC[14,15] and AlN,[16,17] have demonstrated that the cubic NbN grows with the [1 1 1] lattice vector oriented along the hexagonal substrate out-of-plane c-axis. The structural similarities between the rock-salt (δ-phase) NbN and the wurtzite GaN are best observed through the stacking of the cation basal planes, as shown in Fig. 2(a). Wurtzite GaN exhibits ABAB stacking, whereas two possible stacking sequences (ABCA and ACBA) of NbN have equivalent symmetry relationships to GaN.

We confirm the lattice orientation of the NbN relative to the GaN using x-ray diffraction (XRD). The in-plane orientation of the NbN is analyzed using skew symmetric XRD [Fig. 2(b)]. Although the cubic-NbN possesses threefold symmetry about the out-of-plane [1 1 1] lattice vector, an apparent sixfold symmetry of the NbN is observed due to the presence of NbN domains of both possible orientations shown in Fig. 2(a).

A ω rocking curve measurement of the NbN (1 1 1) reflection [Fig. 2(c)] shows that the FWHM of the NbN (1 1 1) reflection for a 46 nm NbN film grown on GaN is 291,” a value that confirms that the NbN is highly crystalline and epitaxial.

We have previously studied the domain structure of NbN[14] and ScN[18] grown on 6H-SiC and have shown that the domains form a periodic array with parallel boundaries. Other reports have shown similar behavior for the growth of NbN on AlN,[16] in which it is demonstrated that there is a correlation between the step/terrace structure of the underlying AlN and domains of the NbN. High-angle annular dark-field (HAADF)-STEM images of a 5.5 nm NbN film on GaN [Fig. 3(a)] show that the NbN is uniform in thickness and that the NbN/GaN interface is atomically sharp.

The center of Fig. 3(b) shows the site of a NbN domain boundary; the stacking of the NbN atomic planes on either side of the boundary is in opposite directions, corresponding to an in-plane rotation of the NbN lattice by 60°. We observe that the boundary in the NbN is coincident with an atomic step in the GaN surface. We interpret this evidence to indicate that, despite the observed

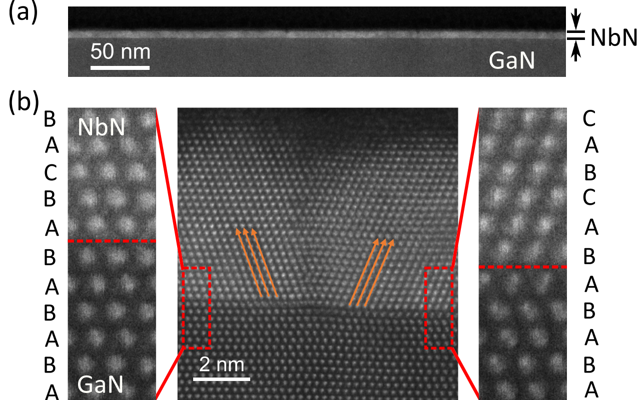

FIG. 3. (a) HAADF-STEM image of a 5.5 nm NbN film on GaN. (b) HAADF-STEM image of the same NbN film at the site of the boundary between two domains of NbN, where the NbN lattice has different orientations on either side of the boundary.

© Author(s) 2022

RHEED oscillations and the atomically terraced surface of the NbN for the first few nanometers, the domains of different orientations form directly at the GaN/NbN interface.

As shown on either side of Fig. 3(b), in both NbN domains, the first two monolayers of NbN continue the stacking sequence of the underlying GaN (i.e., AB stacking in GaN leads to AB stacking for the first two NbN monolayers). However, on either side of the atomic step of the GaN, the GaN surface terminates with a different layer (B layer on the left side and A layer on the right side), causing the NbN stacking direction to be different on either side of the atomic step.

The conclusion that the lattice orientation of the NbN is determined by the surface termination of the GaN opens the possibility that, by engineering of the atomic steps of the GaN surface, the size and orientation of NbN domains could be engineered. For example, reducing the substrate offcut angle can increase the size of the atomic terraces of the GaN surface, and thus increase the size of the NbN domains. Shelton *et al.* have produced atomic-step-free GaN mesas up to 200 μm × 200 μm.[19] Given our observation that domain boundaries in NbN form at the site of the atomic steps on the GaN surface, we hypothesize that single domain NbN films can be grown on atomic-step-free GaN surfaces, such as those demonstrated by Shelton *et al.* Thus, despite the intrinsic symmetry differences between GaN and NbN, the fabrication of domain-free single crystal NbN/GaN heterostructures is plausible, with the size of domain-free material comparable to the atomic-step-free area of the substrate.

B. Electronic properties of the NbN/GaN interface

Figure 4(a) shows the current–voltage (IV) characteristics of the NbN/GaN diode as well as the NbN/GaN device structure used for the IV and capacitance–voltage (CV) measurements. By extracting a linear fit to the forward biased current, we find a turn-on voltage of 0.86 V for the diode. Figure 4(b) shows the room temperature IV characteristics of the NbN/GaN diode in both forward and reverse bias. Strong rectification is clearly observed, and a reverse bias breakdown occurs at ~45 V.

The forward-biased IV curves of NbN/GaN Schottky barrier diodes are fit using the standard thermionic emission model for a diode with a series resistor,[20]

$$I = I_s\left(e^{\frac{q}{\eta kT}(V-IR_s)} - 1\right), \tag{1}$$

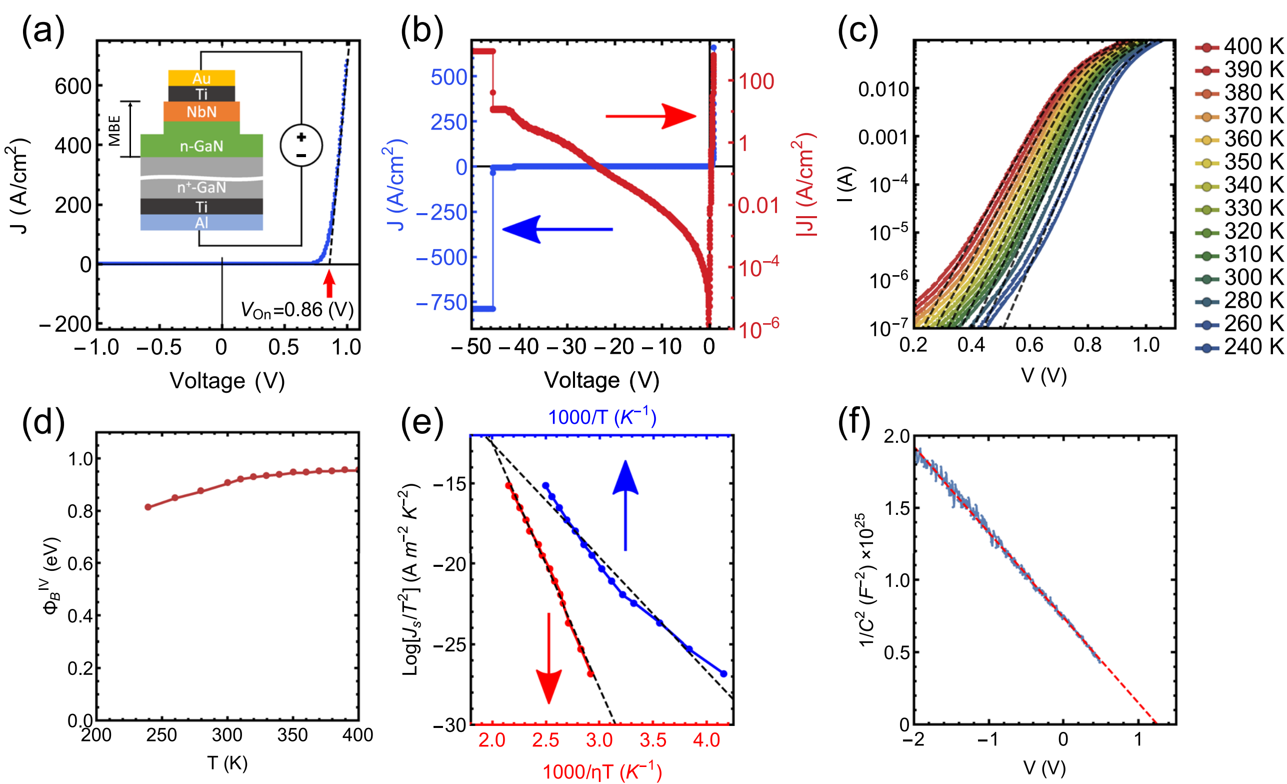

FIG. 4. (a) Room temperature IV characteristics of the NbN/GaN diode. The device structure used for transport measurements is shown in the inset. (b) Room temperature IV characteristics of the NbN/GaN diode showing reverse-bias breakdown around 45 V. (c) Forward-bias IV measurements of NbN/GaN diodes as a function of temperature. The dashed lines represent the best fit to the linear region of the IV curves using a thermionic emission model. (d) Φ_B^{IV} extracted from each IV curve using Eq. (2). (e) Richardson plot and modified Richardson plot for NbN/GaN diodes using values of the saturation current and ideality factor obtained from the forward-bias IV curves. (f) $1/C^2$ vs V obtained from CV measurements of NbN/GaN diodes. The linear fit is used to extract the carrier concentration in the GaN and the NbN/GaN barrier height.

© Author(s) 2022

where q is the elementary charge, η is the ideality factor, k is Boltzmann's constant, T is the temperature, V is the voltage across the diode, I is the diode current, R_s is the series resistance, and I_s is the saturation current given by[20]

$$I_s = A\ A^*\ \exp\left(-\frac{q\Phi_B}{kT}\right), \qquad (2)$$

where A is the diode area, A^* is the Richardson constant, and Φ_B is the Schottky barrier height. From the fitting of each IV curve, I_s, R_s, and η were determined. The theoretically expected value of A^* for n-type GaN is $A^*_{\text{GaN}} = 26.438$ A cm^{-2} K^{-2},[20,21] and using this value, Eq. (2), and the best fit value of I_s, the barrier height Φ_B^{IV} was determined.

Figure 4(c) shows IV curves at various temperatures for a 100 μm diameter circular NbN/GaN diode, as well as the best fit lines using Eq. (1). Figure 4(d) shows the values of Φ_B^{IV} extracted using Eq. (2) and the best fit values of I_s at each temperature. As shown in Fig. 4(d), the values of Φ_B^{IV} determined through this method show a substantial variation as a function of temperature.

An alternative method to determine Φ_B using temperature dependent IV measurements (IVT), which does not rely on the theoretically expected value of A^*, is performed by utilizing a Richardson plot of $1/kT$ vs $\ln(I_s/A)$. By Eq. (2), the slope of the Richardson plot is Φ_B^{IVT} and the y-intercept is A^*.

Figure 4(e) shows the extracted Richardson plot of $1/kT$ vs $\ln(I_s/A)$. We observe that the linear fit to the Richardson plot is quite poor ($R^2 = 0.972$). Similar observations have been reported in previous studies of both Ni/GaN[22] and Sn/Si[23] Schottky barrier diodes. In addition to a curved Richardson plot, such reports show increases in the ideality factor at lower measurement temperatures, which we observe as well. Werner and Güttler[24,25] theoretically demonstrate that such behavior can be well explained by inhomogeneities in the Schottky barrier, and that the flat-band barrier height is extracted from a modified Richardson plot of $1/\eta kT$ vs $\ln(I_s/A)$. As shown in Fig. 4(e), the linear fit to the modified Richardson plot is significantly improved ($R^2 = 0.997$), and we extract a value for the flat-band barrier height, $\Phi_{B_{FB}}^{IVT} = 1.31 \pm 0.02$ eV, using this method.

The presence of inhomogeneities in the Schottky barrier is initially surprising given the low defect density of the bulk GaN substrate, the smooth interface between NbN and GaN, and the highly crystalline nature of the NbN. Werner and Güttler point out that, even for highly uniform interfaces, the statistical distribution of dopant atoms within the space-charge region generate spatial fluctuations in the barrier height.[26] We further hypothesize that domain boundaries in the NbN, which possess significantly greater disorder than the regions within the domains, could contribute to the observed barrier height inhomogeneity. We suggest that further studies could examine work function variations in NbN and other cubic twinned TMNs due to domain boundaries using Kelvin probe force microscopy. Another possible method to investigate the roles of the domain boundaries on the electronic properties of the diodes is to fabricate domain boundary free diodes, either by developing large scale single-domain NbN films or by fabricating nanoscale diodes, thus enabling the fabrication of a diode on a single domain. Due to the variation of the ideality factor with temperature and the excellent fit of a linear model to the modified Richardson plot, we conclude that $\Phi_{B_{FB}}^{IVT}$ extracted from the modified Richardson plot provides a more reliable measurement of the flat-band barrier height than Φ_B^{IV} determined solely using the best fit values of I_s and the theoretically expected value of A^*.

CV measurements were also used to determine the value of the NbN/GaN barrier height. The capacitance at a given bias voltage for a Schottky barrier diode is given by[20]

$$\frac{C}{A} = \sqrt{\frac{q\varepsilon_s N_D}{2V_{bi} - V - kT/q}}, \qquad (3)$$

where C is the capacitance, A is the diode area, ε_s is the semiconductor permittivity, N_D is the donor concentration, and V_{bi} is the built-in voltage. A plot of $(A/C)^2$ vs V, therefore, yields N_D and V_{bi} through the slope and x-intercept, respectively. The Schottky barrier height Φ_B^{CV} is related to V_{bi} by[20]

$$\Phi_B^{CV} = V_{bi} + (kT/q)\ln(N_C/N_D), \qquad (4)$$

where N_c is the effective density of states in the semiconductor conduction band, which for GaN is given by $N_c = 4.3 \times 10^{14} T^{3/2}$ cm^{-3} K$^{-3/2}$.[21]

Figure 4(e) shows the plot of $1/C^2$ vs V for a NbN/GaN diode. From the linear fit ($R^2 = 0.996$) and Eq. (3), we extract $N_D = (4.50 \pm 0.02) \times 10^{16}$ cm^{-3} and $V_{bi} = 1.28$ V. Using Eq. (4), we determine a barrier height $\Phi_B^{CV} = 1.38 \pm 0.01$ eV.

The values of the barrier heights obtained by IVT and CV methods, $\Phi_{B_{FB}}^{IVT}$ and Φ_B^{CV}, respectively, are different by 0.07 eV, a degree of agreement that we feel instills confidence in the results. We hypothesize that transport mechanisms other than thermionic emission, which are not considered in the model used, may lead to an underestimation of the barrier by the IVT method.

III. CONCLUSION AND DISCUSSION

We demonstrate that atomically smooth, epitaxial NbN films with thicknesses of 3 nm and superconducting critical temperature of ~13 K can be grown on GaN by molecular beam epitaxy (MBE). The conductivity and T_c of the thin NbN films are among the highest for NbN films of these thicknesses.[27,28] The growth of NbN shows a transition from layer-by-layer growth mode to island growth mode above a film thickness of between 3 and 6 nm. Using cross-sectional STEM, we demonstrate that the NbN adopts the stacking sequence from the underlying GaN, and therefore, domain boundaries in the NbN are generated at the site of atomic steps in the GaN surface.

This finding has relevance not only for these specific materials but also to NbN grown on other c-plane hexagonal substrates such as 6H-SiC[14] and AlN,[17] and even to other transition metal nitride materials, such as ScN, where similar cubic-twin-domains have been observed.[18] The clear correlation we demonstrate between substrate atomic steps and domain boundaries in the overgrown film presents opportunities to engineer, or even eliminate, the presence of domain boundaries.

Electronic characterization of the NbN/GaN interface allows us to determine the Schottky barrier height at the NbN/GaN interface by IVT and CV measurements to be $\Phi_{B_{FB}}^{IVT} = 1.31 \pm 0.02$ eV and $\Phi_B^{CV} = 1.38 \pm 0.01$ eV, respectively. The work function of NbN, ϕ_{NbN}, has previously been measured to vary as

© Author(s) 2022

function of nitrogen composition between 4.7 eV < ϕ_{NbN} < 4.9 eV.[29] Using Schottky–Mott theory, the expected Schottky barrier height is equal to the difference between the metal work function and the semiconductor electron affinity. Using the electron affinity of GaN, χ_{GaN} = 4.1 eV,[21] and ϕ_{NbN}, the Schottky barrier height for the NbN/GaN junction is predicted by Schottky–Mott theory to be between 0.6eV < Φ_B < 0.8 eV. While this values is close to the value we measure for Φ_B^{IV}, we suspect this may merely be fortuitous, as both $\Phi_{B_{FB}}^{IVT}$ and Φ_B^{CV} measure a significantly larger value for the barrier height, and we believe these measurements are more reliable.

An alternative to Schottky–Mott theory for predicting the barrier height at metal–semiconductor interfaces, which attempts to account for the presence of interface electronic states, is the metal-induced gap states (MIGS) model. Using the MIGS model, the Schottky barrier height Φ_B^{MIGS} is given by[30]

$$\Phi_B^{MIGS} = \Phi_{BP}^n + S_x(X_m - X_s), \tag{5}$$

where Φ_{BP}^n is the n-type branch point energy of the MIGS, S_x is a slope parameter that describes the effect of electronegativity differences on the barrier height, and X_m and X_s are the electronegativities of the metal and semiconductor, respectively. Using measured Schottky barrier height values for several metals on Ga-polar GaN, and Miedema values for electronegativities, Mönch *et al.* extracted the values Φ_{BP}^n = 1.12 ± 0.02 eV and S_x = 0.27 ± 0.02 eV /(Miedemaunit) for GaN.[30] Using these values and the Miedema values for GaN and NbN,[31] wherein the Miedema value is taken to be the geometric mean of the constituent elements for these compounds, we determine the predicted MIGS Schottky barrier height for the NbN/GaN junction to be Φ_B^{MIGS} = 1.10 ± 0.02 eV. We thereby find that the predicted barrier height using the MIGS model and the parameters measured by Mönch for Ga-polar n-GaN is significantly closer to the measured values of $\Phi_{B_{FB}}^{IVT}$ = 1.31 ± 0.02 eV and Φ_B^{CV} = 1.38 ± 0.01 eV than the value of the barrier predicted using the Schottky–Mott model.

Using the measured value of the Schottky barrier height Φ_B^{CV} = 1.38 eV and reported values of the conduction band energy offset between GaN, AlN,[32] and 6H-SiC,[33] we can predict the Schottky barrier heights of NbN/AlN to be 3.04 eV and NbN/6H-SiC to be 1.28 eV. The GaN/InN conduction band offset has been reported to have a value of ΔE_c = 1.68eV, and, given that this is larger than the NbN/GaN Schottky barrier height, it is thus expected that the NbN Fermi level will lie within the conduction band of InN, thereby forming an ohmic contact.[34]

Epitaxial structures integrating metallic and superconducting TMN and III-N semiconductors present pathways to new and improved electronic devices. Essential for realizing these possibilities is an understanding of the growth of TMN/III-N heterostructures, as well as the electronic properties of TMN/III-N interfaces. The large energy barrier between the NbN Fermi-level and GaN conduction band prevents significant interaction between the electronic states at the interface, and thereby superconducting proximity effects should be weak. Interestingly, the Schottky barrier height, and thereby interaction between the electronic states at the interface, could be tuned using InGaN alloys, wherein greater indium composition leads to a reduction of the bandgap and thereby a shrinking Schottky barrier height.

IV. METHODS

NbN and GaN films are grown by plasma-assisted molecular beam epitaxy (PAMBE) using a Veeco GENxplor MBE system in which the base pressure is below 1 × 10^{-10} Torr. Nb is supplied by an electron-beam evaporator; Nb flux is measured using an electron impact energy spectroscopy (EIES) system. Ga flux is supplied by a standard effusion cell. Active nitrogen is supplied using an RF plasma source. Film growth is monitored *in situ* using reflection high energy electron diffraction (RHEED).

To study the growth of NbN on GaN, both single crystal GaN and commercially available hydride vapor phase epitaxy (HVPE) grown GaN on sapphire wafers are used as substrates. Prior to NbN growth, a GaN film of at least 150 nm is grown by MBE to provide a clean surface for NbN nucleation.

We have observed that the growth temperature of NbN on GaN is limited by the decomposition temperature of GaN. As is well known, the growth temperature of GaN by MBE is limited by thermal decomposition of GaN to temperatures below ~800 °C.[35] Given the high melting temperature of NbN, around 2500 °C,[36] the decomposition temperature of GaN is, therefore, only around 35% of the NbN melting temperature. Several attempts were made to nucleate a thin NbN on GaN below the GaN decomposition temperature, and then increase the temperature for the remaining NbN growth above the GaN decomposition temperature; however, this technique did not achieve the intended goal of preventing GaN decomposition, and the resulting film qualities were very poor. Therefore, all NbN films discussed throughout this work were performed at temperatures below the GaN thermal decomposition temperature.

The GaN films were grown in Ga-rich conditions, a typical growth condition for MBE GaN growth. It was discovered that accumulated Ga droplets on the GaN surface severely degraded the NbN film quality, leading to the formation of particulates on the surface that could not be thermally desorbed, which we attributed to the formation of intermetallic Ga–Nb compounds. Therefore, all GaN films were thermally annealed after GaN growth and prior to the nucleation of NbN to remove Ga droplets. NbN was grown in conditions where the active nitrogen flux exceeded the Nb flux by a factor of ~4.

The surface properties of the NbN films were characterized using tapping mode atomic force microscopy (AFM) using an Asylum Research Cypher AFM. Additional structural analysis was performed by preparing TEM cross-sectional samples. HAADF-STEM imaging was performed using an aberration-corrected Titan Themis at an acceleration voltage of 300 keV. High-resolution x-ray diffraction (XRD) characterization of the films was performed using a Malvern Panalytical X'pert Pro system with a Cu Kα1 radiation (1.540 57 Å) x-ray source operated at 45 kV, 40 mA. XRD measurements are performed using a triple axis geometry.

The superconducting transition temperatures of NbN films were measured by performing R vs T measurements in a Quantum Design Physical Property Measurement System (PPMS) system, and T_c is defined as the temperature at which the film resistance goes to half of the normal state resistance.

To characterize the electronic properties of the NbN/GaN interface, Schottky barrier diodes were fabricated and measured using capacitance–voltage (CV) and current–voltage–temperature (IVT) techniques. The structure for the diodes consisted of a 50 nm

© Author(s) 2022

NbN film grown on a 500 nm Si-doped GaN film with a donor concentration of 5×10^{16} cm^{-3} grown on a single crystal n^+-GaN substrate. The diode areas were defined using BCl_3 inductively coupled plasma reactive-ion etching(ICP-RIE). Ti/Au contacts were deposited on the NbN to enable easier probing and wire bonding to the devices. Backside contact to the n^+-GaN substrate was made using a Ti/Al contact.

IVT measurements were performed using 100 μm diameter circular diodes in a Quantum Design PPMS system using an external Agilent B1505A analyzer. Measurements were performed between 400 and 2 K, but for temperatures below ~240 K, the diodes showed increased contribution of non-thermionic currents when forward-biased, as determined by the poor fit of an exponential IV model, and therefore were not used for the IVT analysis.

CV measurements were performed using circular diodes of 20 μm diameter, as it was found that these devices had lower leakage in reverse bias than did larger diameter diodes. CV measurements were performed using a Keithley 4200A-SCS parameter analyzer using a 20 mV amplitude excitation at a frequency of 1 MHz at room temperature.

ACKNOWLEDGMENTS

This work used the CNF, CCMR, and CESI Shared Facilities partly supported by the NSF NNCI program (Grant No. ECCS-1542081), the MRSEC program (Grant No. DMR-1719875), and MRI Grant No. DMR-1338010 and Kavli Institute at Cornell (KIC). We acknowledge funding support from the Office of Naval Research, monitored by P. Maki (Award Nos. N00014-20-1-2176 and N00014-17-1-2414).

AUTHOR DECLARATIONS

Conflict of Interest

The authors have no conflicts to disclose.

DATA AVAILABILITY

The data that support the findings of this study are available from the corresponding author upon reasonable request.

REFERENCES

[1] S. Kim, H. Terai, T. Yamashita, W. Qiu, T. Fuse, F. Yoshihara, S. Ashhab, K. Inomata, and K. Semba, "Enhanced coherence of all-nitride superconducting qubits epitaxially grown on silicon substrate," Commun. Mater. **2**(1), 98 (2021).

[2] Y. Nakamura, H. Terai, K. Inomata, T. Yamamoto, W. Qiu, and Z. Wang, "Superconducting qubits consisting of epitaxially grown NbN/AlN/NbN Josephson junctions," Appl. Phys. Lett. **99**, 212502 (2011).

[3] J. Miller, J. Wright, H. G. Xing, and D. Jena, "All-epitaxial bulk acoustic wave resonators," Phys. Status Solidi A **217**, 1900786 (2020).

[4] V. J. Gokhale, B. P. Downey, D. S. Katzer, N. Nepal, A. C. Lang, R. M. Stroud, and D. J. Meyer, "Epitaxial bulk acoustic wave resonators as highly coherent multi-phonon sources for quantum acoustodynamics," Nat. Commun. **11**(1), 2314 (2020).

[5] B. Saha, S. Saber, G. V. Naik, A. Boltasseva, E. A. Stach, E. P. Kvam, and T. D. Sands, "Development of epitaxial $Al_xSc_{1-x}N$ for artificially structured metal/semiconductor superlattice metamaterials," Phys. Status Solidi B **252**, 251–259 (2015).

[6] B. Saha, G. V. Naik, S. Saber, C. Akatay, E. A. Stach, V. M. Shalaev, A. Boltasseva, and T. D. Sands, "TiN/(Al,Sc)N metal/dielectric superlattices and multilayers as hyperbolic metamaterials in the visible spectral range," Phys. Rev. B **90**, 125420 (2014).

[7] G. V. Naik, B. Saha, J. Liu, S. M. Saber, E. A. Stach, J. M. K. Irudayaraj, T. D. Sands, V. M. Shalaev, and A. Boltasseva, "Epitaxial superlattices with titanium nitride as a plasmonic component for optical hyperbolic metamaterials," Proc. Natl. Acad. Sci. U. S. A. **111**, 7546–7551 (2014).

[8] P. Dang, G. Khalsa, C. S. Chang, D. S. Katzer, N. Nepal, B. P. Downey, V. D. Wheeler, A. Suslov, A. Xie, E. Beam, Y. Cao, C. Lee, D. A. Muller, H. G. Xing, D. J. Meyer, and D. Jena, "An all-epitaxial nitride heterostructure with concurrent quantum Hall effect and superconductivity," Sci. Adv. **7**, eabf1388 (2021).

[9] R. Yan, G. Khalsa, S. Vishwanath, Y. Han, J. Wright, S. Rouvimov, D. S. Katzer, N. Nepal, B. P. Downey, D. A. Muller, H. G. Xing, D. J. Meyer, and D. Jena, "GaN/NbN epitaxial semiconductor/superconductor heterostructures," Nature **555**, 183–189 (2018).

[10] D. Sam-Giao, S. Pouget, C. Bougerol, E. Monroy, A. Grimm, S. Jebari, M. Hofheinz, J.-M. Gérard, and V. Zwiller, "High-quality NbN nanofilms on a GaN/AlN heterostructure," AIP Adv. **4**, 107123 (2014).

[11] N. Tabatabaie, T. Sands, J. P. Harbison, H. L. Gilchrist, and V. G. Keramidas, "Negative differential resistance in AlAs/NiAl/AlAs heterostructures: Evidence for size quantization in metals," Appl. Phys. Lett. **53**, 2528 (1988).

[12] J. P. Harbison, T. Sands, N. Tabatabaie, W. K. Chan, L. T. Florez, and V. G. Keramidas, "Molecular beam epitaxial growth of ultrathin buried metal layers: (Al,Ga)As/NiAl/(Al,Ga)As heterostructures," Appl. Phys. Lett. **53**, 1717–1719 (1988).

[13] B. Saha, A. Shakouri, and T. D. Sands, "Rocksalt nitride metal/semiconductor superlattices: A new class of artificially structured materials," Appl. Phys. Rev. **5**, 021101 (2018).

[14] J. Wright, C. Chang, D. Waters, F. Lupke, R. Feenstra, L. Raymond, R. Koscica, G. Khalsa, D. Muller, H. G. Xing, and D. Jena, "Unexplored MBE growth mode reveals new properties of superconducting NbN," Phys. Rev. Mater. **5**, 024802 (2021).

[15] D. S. Katzer, N. Nepal, D. J. Meyer, B. P. Downey, V. D. Wheeler, D. F. Storm, and M. T. Hardy, "Epitaxial metallic β-Nb_2N films grown by MBE on hexagonal SiC substrates," Appl. Phys. Express **8**, 085501 (2015).

[16] A. Kobayashi, K. Ueno, and H. Fujioka, "Autonomous growth of NbN nanostructures on atomically flat AlN surfaces," Appl. Phys. Lett. **117**, 231601 (2020).

[17] A. Kobayashi, K. Ueno, and H. Fujioka, "Coherent epitaxial growth of superconducting NbN ultrathin films on AlN by sputtering," Appl. Phys. Express **13**, 061006 (2020).

[18] J. Casamento, J. Wright, R. Chaudhuri, H. Xing, and D. Jena, "Molecular beam epitaxial growth of scandium nitride on hexagonal SiC, GaN, and AlN," Appl. Phys. Lett. **115**, 172101 (2019).

[19] C. T. Shelton, I. Bryan, and E. A. Paisley, "Step-free GaN surfaces grown by confined-area metal-organic vapor phase epitaxy," APL Mater. **5**, 096109 (2017).

[20] D. K. Schroder, *Semiconductor Material and Device Characterization*, 3rd ed. (Wiley, 2005), pp. 1–779.

[21] M. E. Levinshtein, S. L. Rumyantsev, and M. Shur, *Properties of Advanced Semiconductor Materials: GaN, AlN, InN, BN, SiC, SiGe* (Wiley, 2001), p. 194.

[22] A. R. Arehart, B. Moran, J. S. Speck, U. K. Mishra, S. P. DenBaars, and S. A. Ringel, "Effect of threading dislocation density on Ni/*n*-GaN Schottky diode *I-V* characteristics," J. Appl. Phys. **100**, 023709 (2006).

[23] Ş. Karataş, Ş. Altindal, A. Türüt, and A. Özmen, "Temperature dependence of characteristic parameters of the H-terminated Sn/p-Si(1 0 0) Schottky contacts," Appl. Surf. Sci. **217**, 250–260 (2003).

[24] J. H. Werner and H. H. Güttler, "Barrier inhomogeneities at Schottky contacts," J. Appl. Phys. **69**, 1522 (1991).

[25] J. H. Werner, H. H. Guttler, and U. Rau, "Barrier inhomogeneities at Schottky contacts: Curved Richardson plots, idealities, and flat band barriers," MRS Online Proc. Libr. **260**, 311 (1992).

[26] J. H. Werner and H. H. Güttler, "Transport properties of inhomogeneous Schottky contacts," Phys. Scr. **1991**, 258 (1991).

[27] A. Semenov, B. Günther, U. Böttger, H. W. Hübers, H. Bartolf, A. Engel, A. Schilling, K. Ilin, M. Siegel, R. Schneider, D. Gerthsen, and N. A. Gippius, "Optical and transport properties of ultrathin NbN films and nanostructures," Phys. Rev. B **80**, 054510 (2009).

© Author(s) 2022

[28]J.-C. Villegier, S. Bouat, P. Cavalier, R. Setzu, R. Espiau de Lamaestre, C. Jorel, P. Odier, B. Guillet, L. Mechin, M. P. Chauvat, and P. Ruterana, "Epitaxial growth of sputtered ultra-thin NbN layers and junctions on sapphire," IEEE Trans. Appl. Supercond. **19**, 3375–3378 (2009).
[29]R. Fujii, Y. Gotoh, M. Y. Liao, H. Tsuji, and J. Ishikawa, "Work function measurement of transition metal nitride and carbide thin films," Vacuum **80**, 832–835 (2006).
[30]W. Mönch, "Electronic properties of ideal and interface-modified metal-semiconductor interfaces," J. Vac. Sci. Technol. B **14**, 2985 (1996).
[31]A. R. Miedema, P. F. de Châtel, and F. R. de Boer, "Cohesion in alloys—Fundamentals of a semi-empirical model," Physica B+C **100**, 1–28 (1980).
[32]A. N. Westmeyer, S. Mahajan, K. K. Bajaj, J. Y. Lin, H. X. Jiang, D. D. Koleske, and R. T. Senger, "Determination of energy-band offsets between GaN and AlN using excitonic luminescence transition in AlGaN alloys," J. Appl. Phys. **99**, 013705 (2006).
[33]N. I. Kuznetsov, A. E. Gubenco, A. E. Nikolaev, Y. V. Melnik, M. N. Blashenkov, I. P. Nikitina, and V. A. Dmitriev, "Electrical characteristics of GaN/6H-SiC n-p heterojunctions," Mater. Sci. Eng., B **46**, 74–78 (1997).
[34]K. Wang, C. Lian, N. Su, D. Jena, and J. Timler, "Conduction band offset at the InN/GaN heterojunction," Appl. Phys. Lett. **91**, 232117 (2007).
[35]N. Grandjean, J. Massies, F. Semond, S. Y. Karpov, and R. A. Talalaev, "GaN evaporation in molecular-beam epitaxy environment," Appl. Phys. Lett. **74**, 1854 (1999).
[36]P. Karl, M. Ubl, M. Hentschel, P. Flad, Z.-Y. Chiao, J.-W. Yang, Y.-J. Lu, and H. Giessen, "Optical properties of niobium nitride plasmonic nanoantennas for the near- and mid-infrared spectral range," Opt. Mater. Express **10**, 2597 (2020).

© Author(s) 2022